JOURNAL OF NANO- AND ELECTRONIC PHYSICS
Vol. **18** No 1, 01029(7pp) (2026)

ЖУРНАЛ НАНО- ТА ЕЛЕКТРОННОЇ ФІЗИКИ
Том **18** № 1, 01029(7cc) (2026)

OPEN ACCESS

REGULAR ARTICLE

Enhanced Solar Cell Performance Using Graphene/TiO_2 Composite as Electron Transport Layer

N. Joshi* ✉, A. Pandey

Department of Electronics and Communication Engineering Jaypee Institute of Information Technology Noida, Uttar Pradesh, India

(Received 08 December 2025; revised manuscript received 20 February 2026; published online 25 February 2026)

This paper presents a simulation-based analysis of a tin-based solar cell and compares it with the lead based solar cell. A comparative study is done to analyze the figures of merit of both the solar cells. In the proposed solar cell device, graphene oxide (GO) is used as the hole transport layer (HTL), titanium oxide (TiO_2) as the electron transport layer (ETL), fluorine doped tin oxide (FTO) as front contact and gold is used as the back contact, which introduces environmentally friendly perovskite solar cells (PSCs). The suggested design uses the environmentally benign $CH_3NH_3SnI_3$ as the absorber layer instead of lead based solar cells, which poses environmental issues because of its lead concentration. Graphene Oxide has excellent mobility and carrier concentration capabilities along with cost-effective production methods. Its strategic use as the HTL increases the PSC's operational efficiency. The performance of tin based solar cell has also been compared with different composites of TiO_2 mixed with graphene and it is observed that the parameters obtained for TiO_2 as ETL layer that are V_{OC} of 0.78 V, a J_{SC} of 32.003 mAcm^{-2}, FF of 79.99 and a PCE of 12.76 %, can be optimized with graphene to the values of V_{OC} of 1.0766 V, J_{sc} of 34.254 mAcm^{-2}, FF of 58.74 and PCE of 21.66%. Impact of CCSE on Power conversion efficiency for various graphene ratios in ETL is analyzed and it is observed that it increases by about 70% of its original value.

Keywords: Solar cell, ETL, Perovskite, Absorber layer.

DOI: 10.21272/jnep.18(1).01029 PACS number: 88.40.H –

1. INTRODUCTION

Perovskite solar cells (PSCs) have emerged as promising candidates for diverse applications, including solar modules, flexible photovoltaic devices, and space-based energy systems. In recent years, extensive experimental investigations and simulation studies have been conducted to optimize their performance and stability. Considerable attention has been directed toward engineering the constituent layers—such as the electron transport layer (ETL), hole transport layer (HTL), cathode, and anode – using a wide range of material systems based on both lead-containing and lead-free perovskite absorbers. The methylammonium lead iodide ($CH_3NH_3PbI_3$) or $MAPbI_3$ absorber layer thickness variation has been simulated from 100 nm to 1500 nm to evaluate various performance parameters [1]. Kesterite materials, graphene oxide and graphene quantum dots have been used as hole transport layer [2-6]. Even porous silicon, Cesium, cadmium and Germanium, manganese, $Cs_2AgBiBr_6$, graphene oxide (GO) and the methylammonium tin tri-iodide, holey graphene, non-fullerenes have been considered as absorber material to increase PSC's operational efficiency [7-10]. An additional film can be added below the absorber layer to increase the efficiency of Copper Indium Gallium selenide (CIGS) solar cells by lowering the interaction losses [11]. The methylammonium lead tri-iodide and rGO/P_3HT based solar cells are analyzed with the help of various characterization techniques to study the film properties [12-13]. The temperature effects on perovskite solar cells have also been observed [14]. Moreover, electron transport layers like CdS, PCBM, ZnO and SnO_2 with graphene oxide are simulated to achieve better power conversion efficiency [6,15]. P3HT/PCBM-Based Organic Photodetectors have also been studied [16]. Additionally, behaviour of tungsten disulfide (WS_2) as HTL for MoS_2 solar cell with ZnSe ETL along with graphene as window layer has been studied [17]. Various organic/inorganic perovskite based solar cells have been designed and analyzed [18-19].

However, physics based understanding of the comparative analysis of lead and tin based solar cells are needed. In lead free designs, $CH_3NH_3SnI_3$ is used as the absorber layer and the use of GO in HTL increases the PSC's operational efficiency [20]. Moreover, we have proposed that along with GO in HTL, GO composite TiO_2 as ETL layer further improves the figure of merits from V_{OC} of 0.78 V, a J_{SC} of 32.003 mAcm^{-2}, FF of 79.99 and a PCE of 12.76% to V_{OC} of 1.0775 V, J_{SC} of 34.254020 mAcm^{-2}, FF of

* Correspondence e-mail: neetu.joshi@mail.jiit.ac.in

Cite this article as: N. Joshi et al., *J. Nano- Electron. Phys.* 18 No 1, 01029 (2026) https://doi.org/10.21272/jnep.18(1).01029

58.66 and PCE of 21.65%. This is because of the better band alignment of GO-$CH_3NH_3SnI_3$-GO+TiO_2 as compared to GO-$CH_3NH_3SnI_3$-TiO_2.

The remainder of this manuscript is structured as follows. Section II presents the device architecture of the PSC and describes the simulation setup employed in SCAPS-1D. Section III provides a comparative performance analysis of lead-based and tin-based perovskite absorbers. Section IV investigates the influence of graphene composition in the TiO_2 ETL. Section V examines the effect of capture cross section of electrons (CCSE) on the power conversion efficiency (PCE) for different graphene ratios in the ETL. It also consolidates the simulation findings and their interpretations. Finally, the Conclusion section summarizes the key outcomes.

2. SOLAR CELL DEVICE STRUCTURE AND SIMULATION SET UP IN SCAPS 1D

This work is done using the simulation tool SCAPS-1D. This tool is suitable for the work done in this manuscript because of its well governed interface, ability to emulate both dark and bright environments. The SCAPS-1D software solves key physical equations such as Poisson's equation, and the continuity equation for holes and electrons to evaluate certain features of solar cells [21].

The first simulated structure shows PSC comprising of GO as the HTL layer, $CH_3NH_3PbI_3$ as the active layer, TiO_2 as the ETL layer and FTO as front contact as shown in Fig. 1 [1,18]. In the second structure, the absorber material is changed to $CH_3NH_3SnI_3$, all other layers remaining the same [18].

Table 1 – Material properties for PSC layers [1, 2, 18, 19]:

Properties	**Front Contact**	**ETL**	**Absorber Layer**		**HTL**
	FTO	TiO_2	$CH_3NH_3PbI_3$	$CH_3NH_3SnI_3$	GO
Thickness (μm)	0.04	0.1	0.2	0.45	0.03
Bandgap (eV)	3.5	3.26	1.5	1.3	3.25
Affinity (eV)	4	4	3.9	4.17	1.9
Dielectric permittivity	9	10	10	10	3
DOS_{CB} (cm^{-3})	2.2E18	1E21	8E20	1E19	2.2E21
DOS_{VB} (cm^{-3})	1.8E19	2E20	8E19	1E19	1.8E21
u_e (cm^2/Vs)	20	20	10	5	100
u_h (cm^2/Vs)	10	10	10	20	300
Acceptor concentration (cm^{-3})	0	0	0	0	1E16
Donor concentration (cm^{-3})	1E19	1E19	1E15	1E15	0

Table 1 lists the input parameters to simulate the initial structure, including bandgap E_g, thickness d, electron affinity χ, dielectric permittivity $\in_r$, conduction band and valence band effective density of states N_C and N_V, donor concentration N_D, and defect concentration N_t. The device structure was simulated under AM 1.5 G illumination at a temperature of 300 K and a 107 cm/s thermal velocity for both electrons and holes. Moreover, the work function of back contact is taken as 5.1 eV. The cell structures involved are FTO/TiO_2/$CH_3NH_3PbI_3$/GO/Au and FTO/TiO_2/$CH_3NH_3SnI_3$/GO/Au.

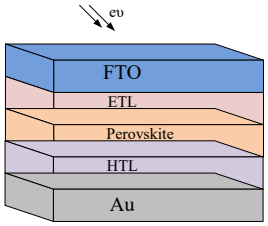

Fig. 1 – Configuration of PSC

Fig. 1 presents the simulated device architecture of the perovskite solar cell, showing the layered structure with FTO as the front contact, TiO_2 as ETL, $CH_3NH_3PbI_3$/$CH_3NH_3SnI_3$ as absorber, GO as HTL, and Au as the back contact. The configuration highlights a planar structure optimized for simulation in SCAPS-1D. The arrangement confirms standard PSC stacking with emphasis on GO as a hole transport layer and the environmentally friendly substitution of Sn-based absorber in place of Pb. The structure sets the basis for comparing lead- and tin-based devices in later figures.

3. COMPARATIVE PERFORMANCE ANALYSIS OF LEAD AND TIN BASED PSC

The two PSC structures are simulated with lead and tin based absorber layers. The layer parameters are given in Table 1. Their comparative analysis is presented in this section. The first PSC structure analyzed is FTO/TiO_2/$CH_3NH_3PbI_3$/GO/Au. The *J-V* plot shows that the lead-based PSC achieves an open-circuit voltage of 1.196 V, a short-circuit current density (J_{sc}) of 18.65 mA/cm^2, and a fill factor (FF) of 59.21 with a power conversion efficiency (PCE) of 13.21 %. The quantum efficiency spectrum confirms efficient photo-response across the visible range, with relatively stable absorption. The comparatively high V_{OC} compensates for the modest J_{sc}, contributing to the observed efficiency.

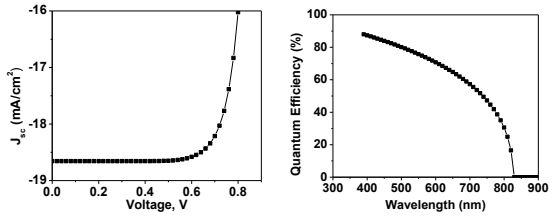

(a) (b)

Fig. 2 – (a) J_{sc} and (b) Quantum efficiency of lead based solar cell

Next simulated structure shows PSC comprising of graphene oxide as the HTL layer, $CH_3NH_3SnI_3$ as the active layer, TiO_2 as the ETL layer and fluorine doped tin oxide (FTO) as front contact is used in this simulation [18]. As shown in Fig. 3, the Sn-based PSC shows a V_{OC} of 0.78 V, which is significantly lower than the Pb-based

device. However, the J_{sc} increases to 32.00 mA/cm^2, nearly double that of the lead cell. The FF improves to 79.99, demonstrating reduced series resistance and better carrier transport. Despite the high J_{sc} and FF, the low V_{OC} limits the efficiency to 12.76%. The quantum efficiency spectrum exhibits broader current generation capability, reflecting better light absorption but also higher recombination losses reducing V_{OC}.

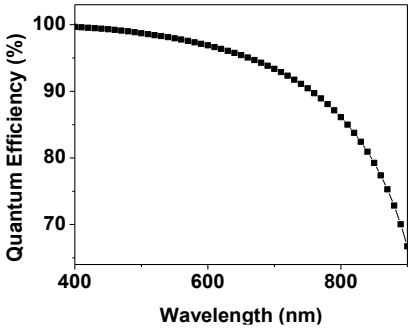

Fig. 3 - Quantum efficiency of tin based solar cell

Table 2

	V_{OC} (V)	J_{SC} (mAcm^{-2})	FF	PCE (%)
Pb	1.196	18.655144	59.21	13.21
Sn	0.78	32.003766	79.99	12.76

We observe that lead based PSC structure shows better PCE as compared to tin based PSC. However, lead based solar cells pose health hazards and environmental issues because of the lead content in the absorber layer. Therefore, in the following work, the environmentally friendly alternative that is, tin based solar cell is explored.

4. IMPACT OF GRAPHENE COMPOSITION IN TIO_2 AS ETL LAYER

The graphene composition in TiO_2 changes its overall behavior as the ETL layer. With the optimal use of TiO_2+Gr nanocomposite as the ETL, carrier transport within the layer improved and resulted in an increase in efficiency.

There are various scalable and non-scalable methods to obtain industrial range graphene/GO. It can be manufactured with the help of various cost-effective production methods [22]. As shown in Fig.4, scalable methods include liquid phase exfoliation or oxidative exfoliation whereas non-scalable methods involve mechanical exfoliation or CVD. The figure illustrates scalable (liquid phase and oxidative exfoliation) and non-scalable (mechanical exfoliation, CVD) synthesis routes for GO. The scalable methods align with industrial feasibility, while non-scalable methods suit laboratory studies. This provides a justification for considering GO in ETL/HTL layers due to ease of production and cost-effectiveness.

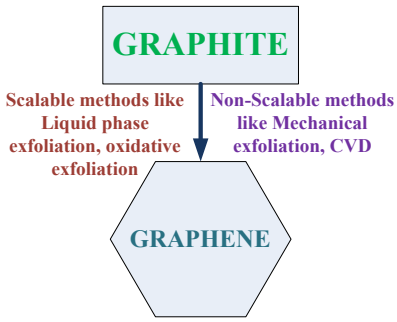

Fig. 4 – Cost-effective production of GO

To analyze the impact of graphene nanocomposite ETL layer on the performance metrics of the perovskite solar cell, the following configurations were simulated and figure of merits were compared. In the layered structure FTO/ETL/ $CH_3NH_3SnI_3$/GO/Au, ETL layer is TiO_2+Gr (x %), where x is varied as 0, 0.5, 1, 1.5, 3, 5, 10, 20. The material properties of TiO_2 and graphene composites are given in Table 3.

Table 3 – Material properties for TiO_2 and graphene composites [19, 23, 24]

Properties	TiO_2 (x = 0.5)	TiO_2 (x = 0.5)	TiO_2+1 (x = 1)	TiO_2 (x = 1.5)	TiO_2 (x = 3)	TiO_2 (x = 5)	TiO_2 (x = 10)	TiO_2 (x = 20)
Thickness (μm)	0.1	0.1	0.1	0.1	0.1	0.1	0.1	0.1
Bandgap (eV)	3.26	2.98	2.91	2.85	3.24	3.1	2.7	2.4
Affinity (eV)	4	4.06	4.16	4.21	4.26	4.31	4.28	4.31
Dielectric permittivity	10	6.8	7.3	7.9	8.4	8.9	7.5	7.8
DOS_{CB} (cm^{-3})	1E21	1E18	1E18	1E18	1E18	1E18	1E19	1E19
DOS_{VB} (cm^{-3})	2E20	1E19	1E19	1E19	1E19	1E19	1E19	1E19
u_e (cm^2/Vs)	20	10	25	125	225	300	325	350
u_h (cm^2/Vs)	10	10	25	125	225	300	325	350
Acceptor concentration (cm^{-3})	0	0	0	0	0	0	0	0
Donor concentration (cm^{-3})	1E19	5E17	5E17	5E17	5E17	5E17	5E18	5E18

The output parameters vary with the percentage of graphene in TiO_2. These variations for V_{OC}, J_{SC}, FF and η are shown in Fig. 5. The plots reveal that increasing graphene concentration in TiO_2 up to ~ 1.5% results in significant improvements in V_{OC} (up to ~ 1.25 V), stable Jsc (~ 34.25 mA/cm^2), and optimized PCE (~ 21.66 %). Beyond 5-20 %, the parameters stabilize with marginal changes. FF decreases when graphene is added, falling

from ~ 80 % in pristine TiO_2 to ~ 58 % in composites, but efficiency still improves due to gains in V_{OC} and J_{SC}. Thus, TiO_2+1.5 %Gr emerges as the optimum ETL composition.

Further, the variations of quantum efficiency with wavelength are shown in Fig. 6 for various ratios of graphene in TiO_2. The spectra demonstrate that adding graphene enhances quantum efficiency across the visible spectrum, particularly in the 400-700 nm range. The improvement is most pronounced for the 1.5 % graphene composite, consistent with the PCE enhancement observed in Fig. 5. Excessive graphene ratios (> 10 %) do not further improve spectral response, confirming the existence of an optimum doping level.

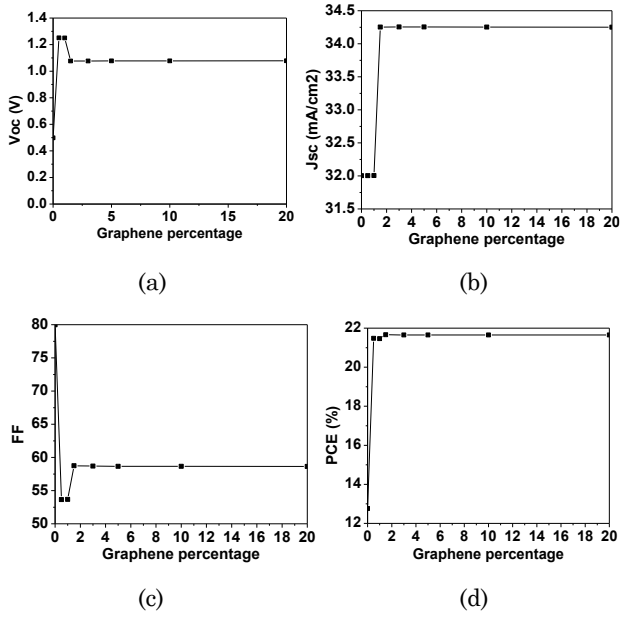

Fig. 5 – Variation in V_{OC}, J_{SC}, *FF* and PCE with the percentage of graphene in TiO_2

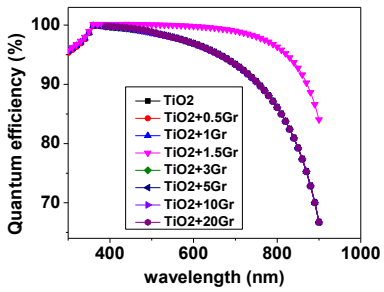

Fig. 6 – Quantum efficiency vs wavelength for various ratios of graphene in ETL

Further, PSC structure without HTL-GO layer has been analyzed. The impact of elimination of the GO layer on various output parameters can be visualized from Fig. 7 as compared to the results shown for PSC structure with HTL-GO layer as shown in Fig. 5. As compared to the output when the GO layer is used as HTL as shown in Fig. 5(d), it can be observed that the efficiency decreases. The comparison demonstrates that incorporating GO as the HTL significantly enhances device performance. With GO, both V_{OC} and *FF* improve (Fig. 5(a), (c) respectively), reflecting reduced interfacial recombination and more effective hole extraction. Jsc remains nearly constant when compared to Fig. 5(b), as absorption is unchanged, but collection efficiency is slightly improved. The overall PCE is higher with GO in Fig. 5(d), confirming its essential role as a selective transport layer. When GO is removed, the absence of a proper HTL leads to severe interfacial recombination, thereby lowering V_{OC} and *FF*, and in turn reducing efficiency.

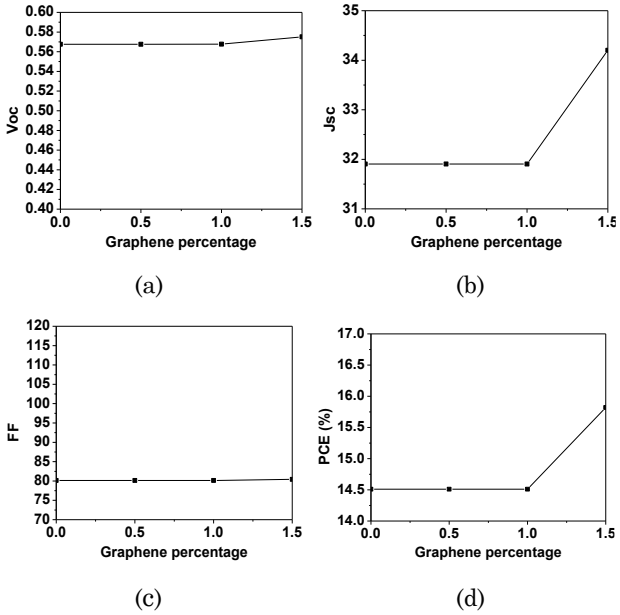

Fig. 7 – Impact of GO on V_{OC}, J_{SC}, *FF* and PCE

5. IMPACT OF CCSE ON POWER CONVERSION EFFICIENCY FOR VARIOUS GRAPHENE RATIOS IN ETL

In solar cells, the capture cross-section of electrons (and holes) (CCSE) significantly impacts the power conversion efficiency (PCE). A smaller capture cross-section generally leads to better PCE, as it reduces carrier recombination, thus increasing the lifetime of photogenerated carriers and enhancing the efficiency of the solar cell [25]. In this section, CCSE is varied at the GO/*i*-layer $CH_3NH_3SnI_3$ and i-layer $CH_3NH_3SnI_3/TiO_2$ layer interfaces. Its PCE value changes with CCSE at the interfaces.

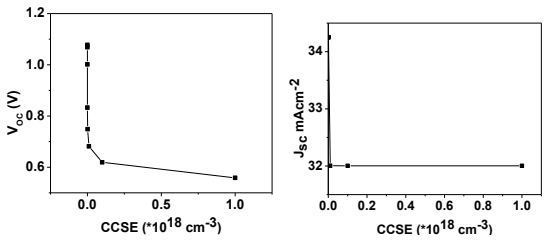

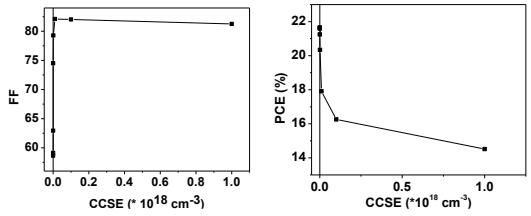

Fig. 8 – Impact of CCSE on V_{OC}, J_{SC}, *FF* and PCE

Therefore, with the observed composites of tin oxide, different values of PCE have been obtained. As the value of CCSE decreases, PCE increases and becomes constant at 21.65 %. As apparent from Fig. 8, V_{OC} and J_{SC} also increase and *FF* decreases with decrease in CCSE, reaching to optimal values. The Gr-doped ETL improves device performance by lowering the energy threshold for electron transmission and reducing coupling loss. This leads to an amalgamation of optical and electrical upgrades, improving energy alignments with respect to the absorber layer and ETL-FTO junction. It reduces series resistance, increasing V_{OC}, *FF*, and overall PCE.

Band Diagram Comparison with TiO_2 Ratio

The band diagrams illustrate the effect of graphene incorporation on band alignment as shown in Fig. 9. With increasing graphene ratios, conduction band edge alignment improves, reducing energy barriers for electron transport. Up to 1.5 % graphene, the alignment is optimal, facilitating efficient carrier extraction. At higher graphene loadings (10-20 %), band offsets distort slightly, offering no further benefit, consistent with Figs. 5 and 6.

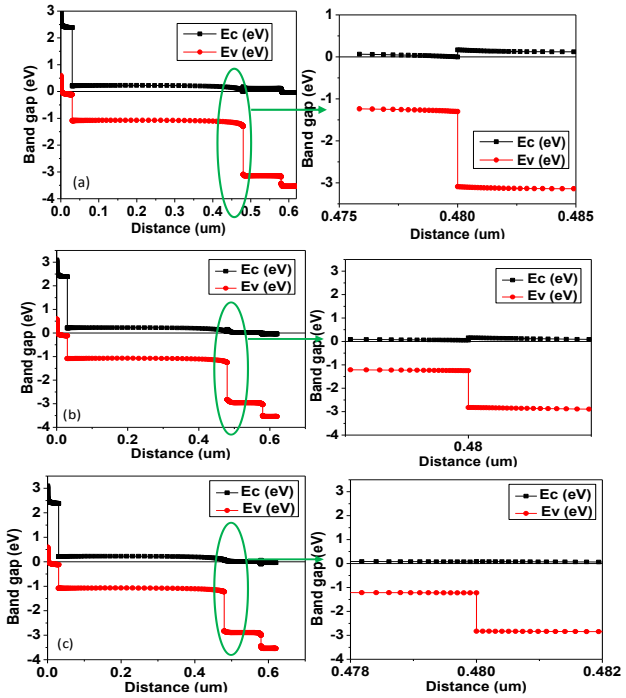

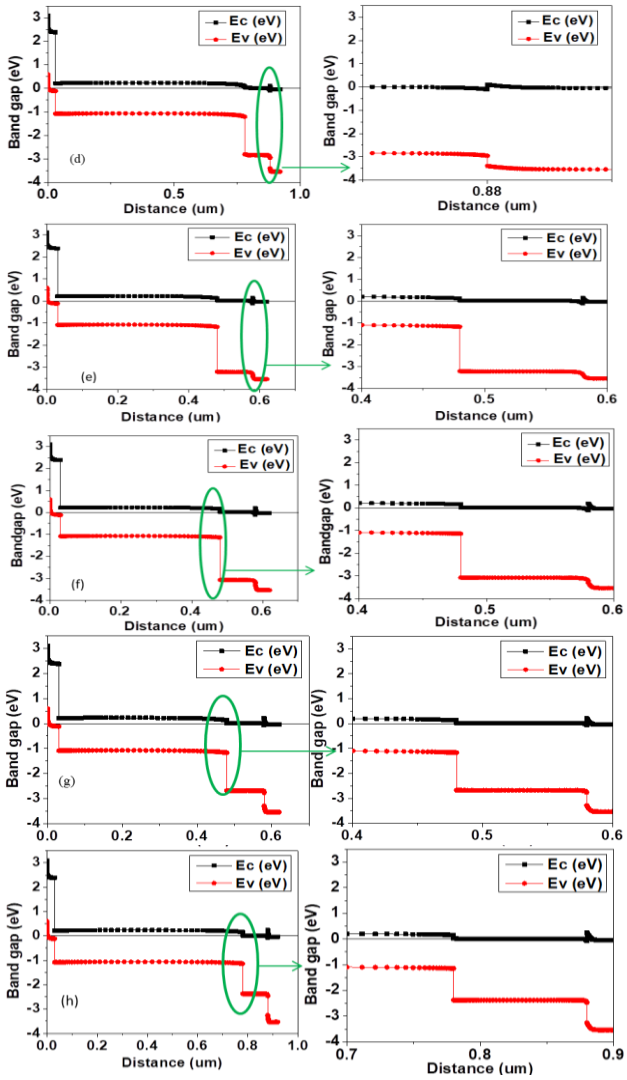

Fig. 9 – Variation of Band gap with distance for (a) TiO_2 (b) TiO_2+0.5% graphene composite (c) TiO_2+1% graphene composite (d) TiO_2+1.5% graphene (e) TiO_2+3% graphene (f) TiO_2+5% graphene (g) TiO_2+10% graphene (h) TiO_2+20% graphene

Following comparative Table 4 summarizes how the Figures of Merits vary with increasing GO/graphene composition in TiO_2 ETL, based on the references compared with our work.

CONCLUSION

This paper shows the comparative analysis of lead and tin based solar cells. Due to environmentally benign nature of tin based solar cell, we have further explored a graphene based FTO/TiO_2/$CH_3NH_3SnI_3$/GO/Au solar cell. Its performance has also been compared with three different composites of TiO_2 mixed with graphene and it is observed that the parameters obtained for pristine undoped TiO_2 as ETL layer are V_{OC} of 0.78 V, a J_{SC} of 32.003 mAcm^{-2}, FF of 79.99 and a PCE of 12.76 % can be optimized with 1.5 % graphene-TiO_2 composite to the best

optimized values of V_{OC} of 1.0766 V, *Jsc* of 34.25 mAcm^{-2}, FF of 58.74 and PCE of 21.66%. PSC structure without HTL-GO has been analyzed. The PCE is higher with GO establishing the role of HTL-GO as selective transport layer. Impact of CCSE on Power conversion efficiency for various graphene ratios in ETL is analyzed and it is observed that it increases by 69.75 % of its original value. The band diagram comparison for different composites of TiO_2 mixed with graphene has also been observed showing optimal band-alignment of TiO_2+1.5 % Gr composite.

Table 4 – Variation of Device Parameters with Graphene/GO Composition in TiO_2 ETL

	Device Structure	Graphene/GO in TiO_2 ETL	V_{OC} (V)	*Jsc* (mA/cm^2)	*FF* (%)	PCE (%)	Notes
This Work (Simulated)	FTO/TiO_2/$CH_3NH_3SnI_3$/GO/Au	0% (pristine TiO_2)	0.78	32	79.99	12.76	Baseline Sn-based PSC
This Work (Simulated)	Same	0.5% Gr	1.2508	32	53.64	21.48	V_{OC} jumps; PCE nearly doubles
This Work (Simulated)	Same	1% Gr	1.2497	32.01	53.67	21.46	Similar to 0.5% case
This Work (Simulated)	Same	1.5% Gr	1.0766	34.25	58.74	21.66	Optimum PCE in simulation
This Work (Simulated)	Same	3% Gr	1.0768	34.25	58.7	21.65	Stable efficiency
This Work (Simulated)	Same	5% Gr	1.0775	34.25	58.66	21.65	No further gain
This Work (Simulated)	Same	10% Gr	1.0773	34.25	58.66	21.65	Performance saturates
This Work (Simulated)	Same	20% Gr	1.0779	34.25	58.65	21.66	Stable at high graphene
Ref 19	FTO/TiO_2/$RbGeI_3$/NiO/Au	0%	0.9126	31.59	–	24.91	Baseline $RbGeI_3$ device
Ref 23	rGO/TiO_2-based cell	3–5% rGO	–	–	–	~4	Very low efficiency
Ref 24	TiO_2/Gr nanocomposite ETL	10% Gr	–	–	–	17.01 (from 14.0)	17.8% improvement due to mobility
Ref 24	TiO_2/Gr nanocomposite ETL	20% Gr	–	–	–	~17	Performance stable, not strongly enhanced

REFERENCES

1. S. Sakib, M. Yusof, M. Noor, M.R. Salim, A.S. Abdullah, A.I. Azmi, M.H. Ibrahim, M.H. Ibrahim, *Mater. Today: Proc.* **80**, 1022 (2023).
2. S. Jakalase, A. Nqombolo, E.L. Meyer, M.A. Agoro, N. Rono, *Nanomaterials* **14**, 2016 (2024).
3. G.G. Njema, J.K. Kibet, S.M. Ngari, *Next Res.* **1**, 100055 (2024).
4. M. Panachikkool, E.T. Aparna, P. Asaithambi, T. Pandiyarajan, *Sci. Rep.* **15**, 100 (2025).
5. L. Moulaoui, O. Bajjou, Y. Lachtioui, A. Najim, M. Archi, K. Rahmani, B. Manaut, *J. Electron. Mater.* **52**, 7541 (2023).
6. M.A. Saifee, F.F.A. Khan, J. Ali, M.A. Khan, M. Shahid Khan, *Eng. Res. Express* **7**, 015003 (2025).
7. M.A. Saifee, M. Ali, F.F.A. Khan, A.K. Srivastava, J. Ali, M.S. Khan, *J. Opt* (2025).
8. A. Najim, L. Moulaoui, A. Laassouli, O. Bajjou, K. Rahmani, *Elect. Eng.* **107**, 7657 (2024).
9. T.I. Taseen, M. Julkarnain, A. Zafor, M.T. Islam, *Heliyon* **10**, e23197 (2024).
10. N. Fauji, Kardiman, V. Efelina, M.F. Hakim, F.C. Suci, R. Hanif, I.N. Gusniar, E. Widianto, *J. Electron. Mater.* **53**, 1539 (2024).
11. D. Fatihi, M.P. Bhandari, S. Golovynskyi, K. Abderrafi, R. Adhiri, *Semiconductor Physics, Quantum Electronics & Optoelectronics* **27** No 3, 337 (2024).
12. S. Rabhi, K. Sekar, K. Kalna, Y.I. Bouderbala, N. Bouri, N. Oueldna, N. Belbachir, K. Dadda, M.S. Aida, N. Attaf, *Opt. Quant. Electron.* **56**, 1372 (2024).
13. A. Najim, L. Moulaoui, A. Bakour, O. Bajjou, K. Rahmani, *J. Opt.* (2024).
14. A. Mortadia, Y. Tabbaib, E. El Hafidi, H. Nasrellah, E. Chahid, M. Monkade, R. El Moznine, *Clean. Eng. Technol.* **24**, 100876 (2025).
15. F.B. Sumona, M. Kashif, H. Bencherif, N.A. Mahmud, A.A.A. Bahajjaj, S. Shafqat, *Opt. Quant. Electron.* **56**, 1619 (2024).

16. A.S. Alali, M. Oduncuoglu, F. Touati, *Nanomaterials* **14**, 1146 (2024).
17. A. Rahmoune, O. Babahani, *J. Opt*, (2024).
18. T.K. Priya, P. Deb, A. Choudhury, *Optik* **316**, 172051 (2024).
19. I.B.A. Ghani, M. Khalid, H. Yan, Y.E. Arfaoui, B. Nawaz, J. Wang, *Optik* **320**, 172116 (2025).
20. A.K. Chaudhary, S. Verma, R.K. Chauhan, *Optik* **295**, 171469 (2023).
21. M. Burgelman, K. Decock, S. Kheli, A. Abass, *Thin Solid Films* **535**, 296 (2013).
22. Y. Nishina, *ACS Nano* **18**, 49 (2024).
23. A. Merazga, J. Al-Zahrani, A. Al-Baradi, B. Omer, A. Badawi, S. Al-Omairy, *Funct. Mater. Lett.* **12** No 4, 1950052 (2019).
24. M. Dadashbeik, D. Fathi, M. Eskandari, *Sol. Energy* **207**, 917 (2020).
25. A.S. Chouhan, N.P. Jasti, S. Avasthi, *Mater. Lett.* **221**, 150 (2018).

Покращена продуктивність сонячних елементів з використанням композиту графен/TiO2 як шару електронного транспорту

N. Joshi, A. Pandey

Department of Electronics and Communication Engineering Jaypee Institute of Information Technology Noida, Uttar Pradesh, India

У цій статті представлено аналіз сонячного елемента на основі олова, заснований на моделюванні, та його порівняння із сонячним елементом на основі свинцю. Проведено порівняльне дослідження для аналізу показників ефективності обох сонячних елементів. У запропонованому пристрої сонячного елемента оксид графену (GO) використовується як шар діркового переносу (HTL), оксид титану (TiO_2) як шар електронного переносу (ETL), легований фтором оксид олова (FTO) як передній контакт, а золото використовується як задній контакт, що робить його екологічно чистим перовскітним сонячним елементом (PSC). У запропонованій конструкції використовується екологічно безпечний $CH_3NH_3SnI_3$ як поглинальний шар замість сонячних елементів на основі свинцю, що створює екологічні проблеми через концентрацію свинцю. Оксид графену має чудову мобільність та можливості концентрації носіїв заряду, а також економічно ефективні методи виробництва. Його стратегічне використання як HTL підвищує експлуатаційну ефективність PSC. Продуктивність сонячних елементів на основі олова також порівнювали з різними композитами TiO_2, змішаними з графеном, і спостерігали, що параметри, отримані для TiO_2 як шару ETL, а саме: V_{OC} 0,78 В, J_{SC} 32,003 мАсм$^{-2}$, *FF* 79,99 та PCE 12,76 %, можуть бути оптимізовані з графеном до значень V_{OC} 1,0766 В, J_{SC} 34,254 мАсм$^{-2}$, *FF* 58,74 та PCE 21,66 %. Було проаналізовано вплив CCSE на ефективність перетворення енергії для різних співвідношень графену в ETL, і спостерігалося, що вона збільшується приблизно на 70 % від початкового значення.

Ключові слова: Сонячний елемент, ETL, Перовскіт, Поглинальний шар.